XIV Fluidization by lift of 300 circular particles in plane Poiseuille flow by DNS

DISCARD THIS PAGE (only used to generate table of contents)

page break →

- **Case 4: : η = 0.05 poise, $R_G = 9.81/\eta^2 = 3.92\times10^4$**

Figure XIV.22 gives the height of the center of gravity of 300 particles in a liquid with $\eta = 0.05$ poise as a function of $R = 6\overline{p}/\eta^2 = 2400\overline{p}$. Snapshots of the evolution to full fluidization are shown in figures XIV.23 to XIV.28. Notice the overshoot in the bed height at early times. The final bed height is an increasing function of $\overline{p}$ (or R). Data for the simulation after the bed settles down to its final height is shown in table XIV.4.

*Table XIV.4. Data for the forward motion of a fluidized suspension of 300 particles after the bed has fully inflated and the average height $\overline{H}$ of all particles has stopped increasing (η = 0.05). $\overline{H} = \overline{H}_0 = 2.65$*d *at* t = *0. $\overline{U}$ and $\overline{\Omega}$ are the average velocity and angular velocity of the particles.*

R	G	$\overline{p}$	$\overline{H}$	$\overline{U}$	$\overline{\Omega}$
240	16.35	0.1	2.83	1.81	0.18
480	8.18	0.2	3.03	4.51	0.46
960	4.09	0.4	3.19	8.67	0.83
1200	3.27	0.5	3.25	10.84	1.07
1680	2.34	0.7	3.41	18.63	1.78
2400	1.64	1.0	3.60	27.13	2.56

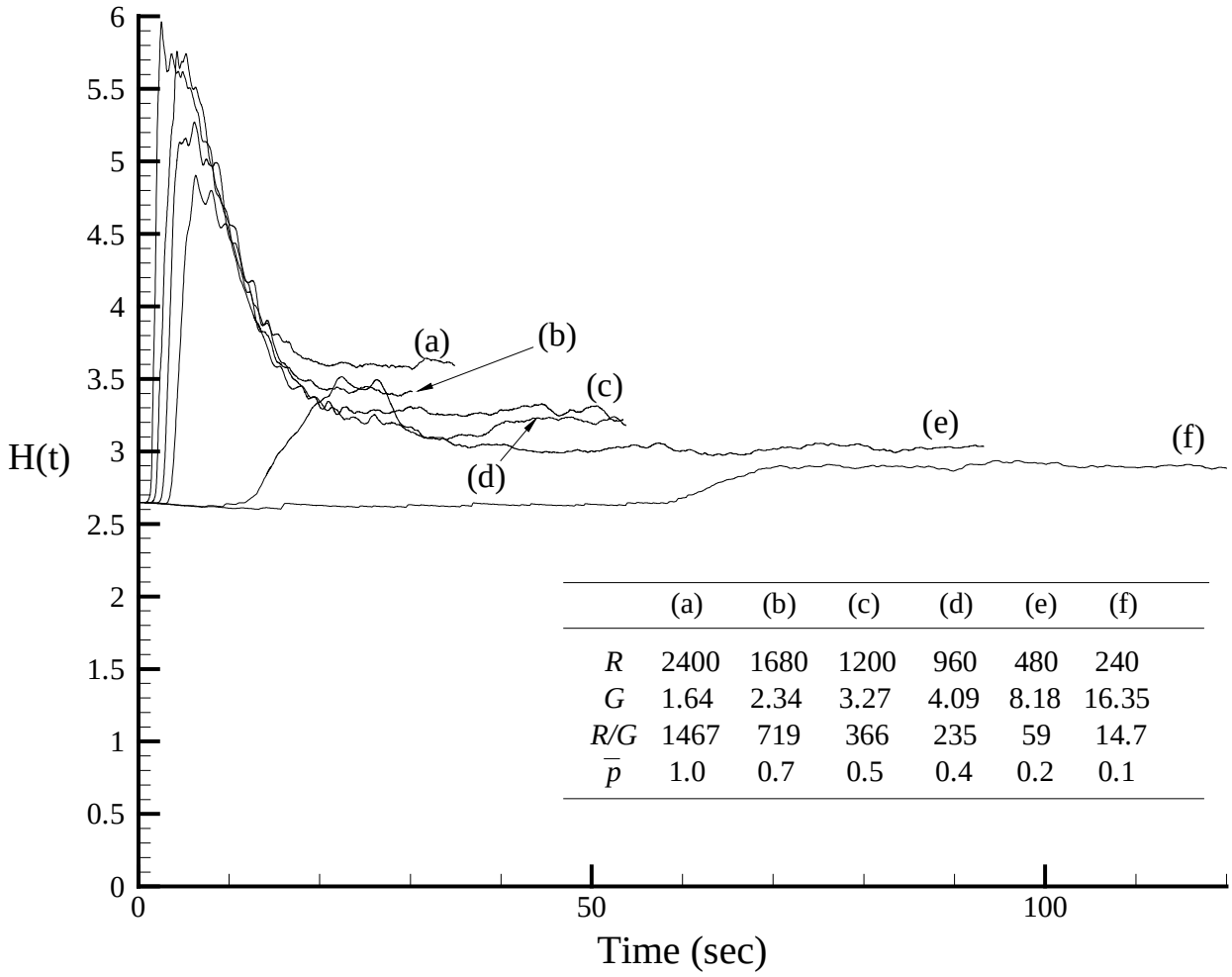

	(a)	(b)	(c)	(d)	(e)	(f)
R	2400	1680	1200	960	480	240
G	1.64	2.34	3.27	4.09	8.18	16.35
R/G	1467	719	366	235	59	14.7
$\overline{p}$	1.0	0.7	0.5	0.4	0.2	0.1

Figure XIV.22. Rise curves for the center of gravity of 300 circular particles fluidized by lift (fluid viscosity = 0.05 poise, $R_G = 9.81/\eta^2 = 3924$, $\overline{p}$ is in dynes/cm^2). Notice the overshoot at early times. The final bed height is an increasing function of $\overline{p}$. The bed is fully fluidized when the rise curves level off. The time to full fluidization is longer when the Reynolds number is smaller.

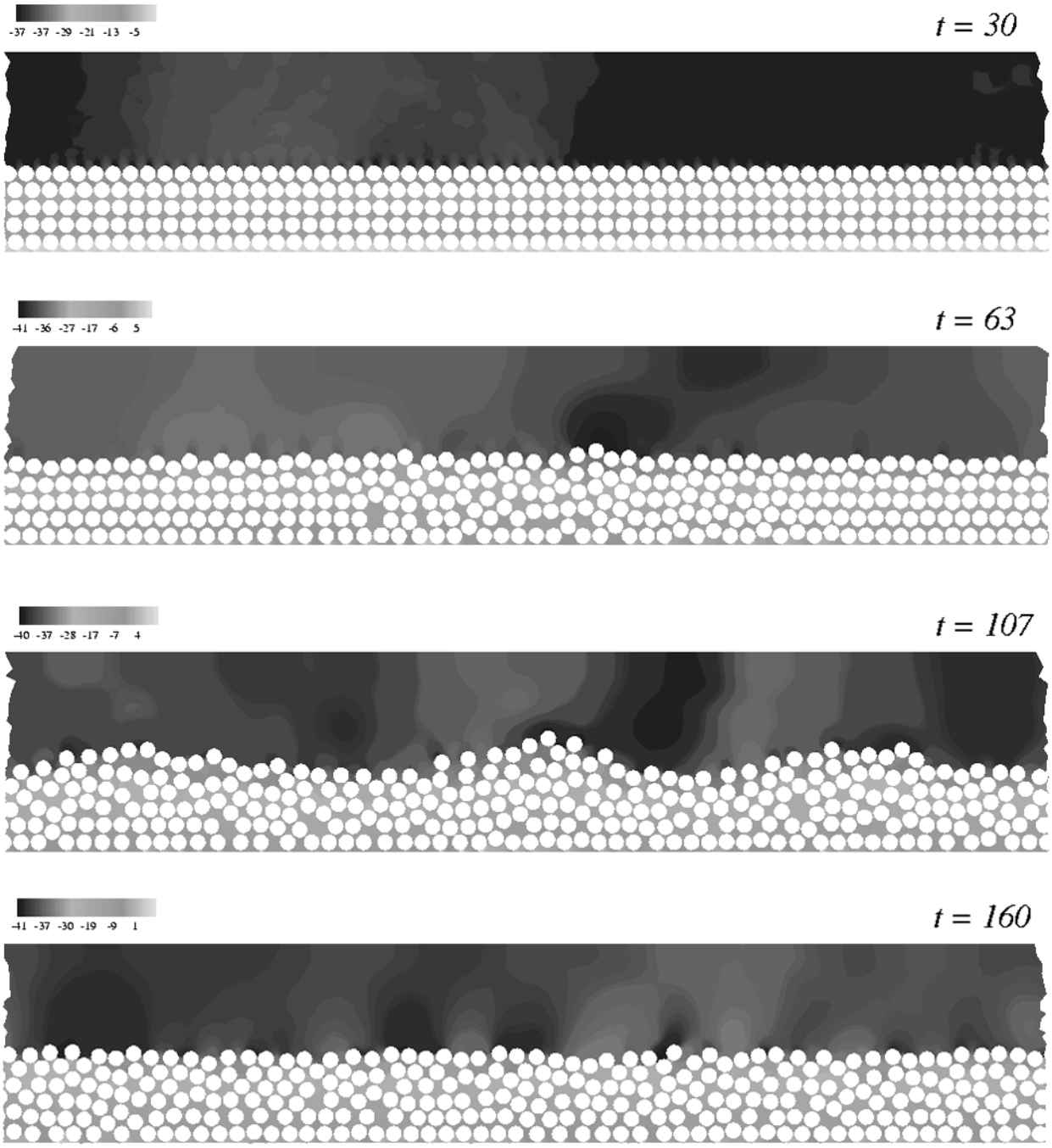

Figure XIV.23. Fluidization of 300 particles (η = 0.05 poise, R = 240, G = 16.35). Flow is from left to right. The qualitative features of fluidization by lift are as in the case η = 0.1 (see figure XIV.39).

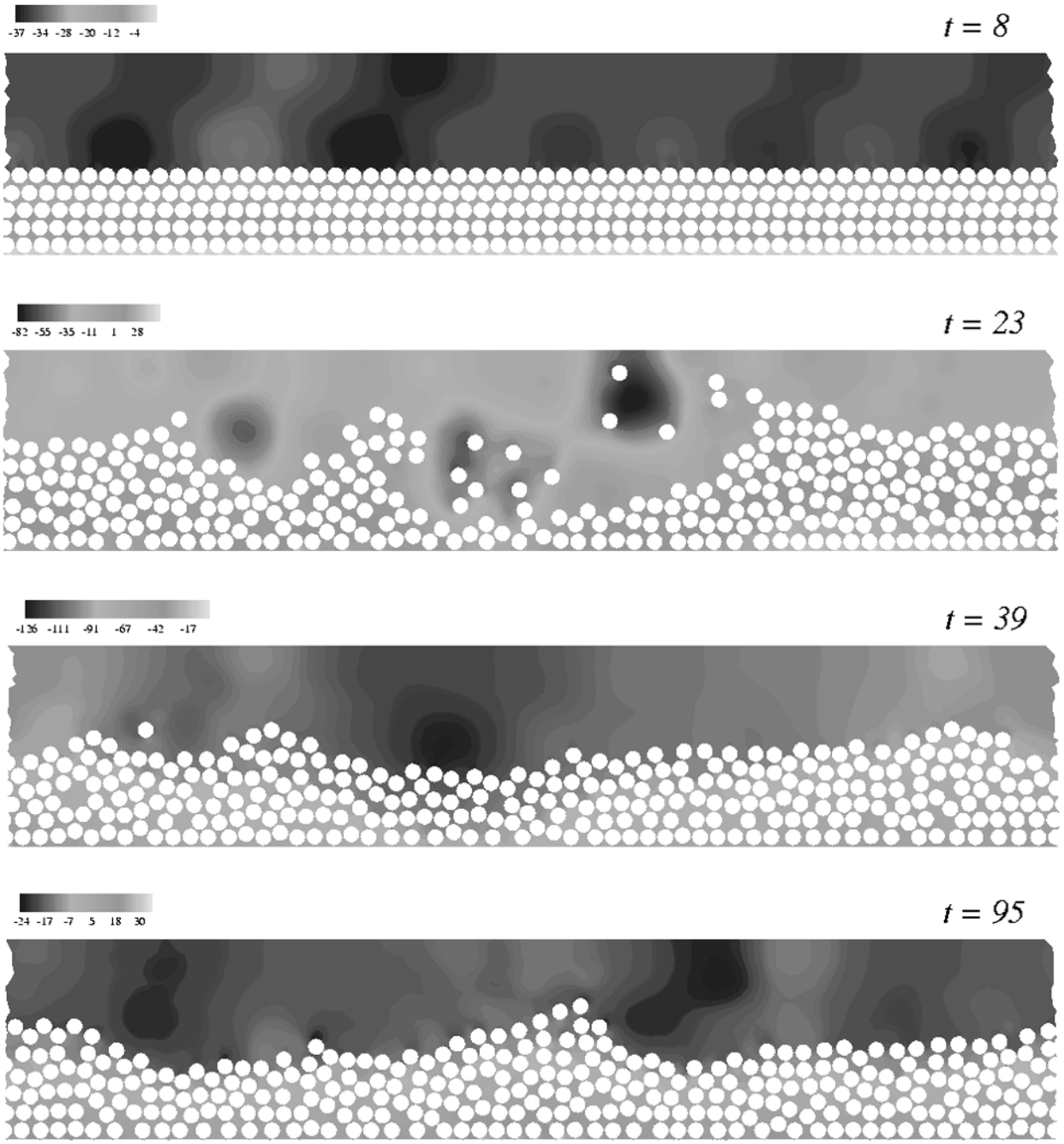

Figure XIV.24. Fluidization of 300 particles (η = 0.05 poise, R = 480, G = 8.18).

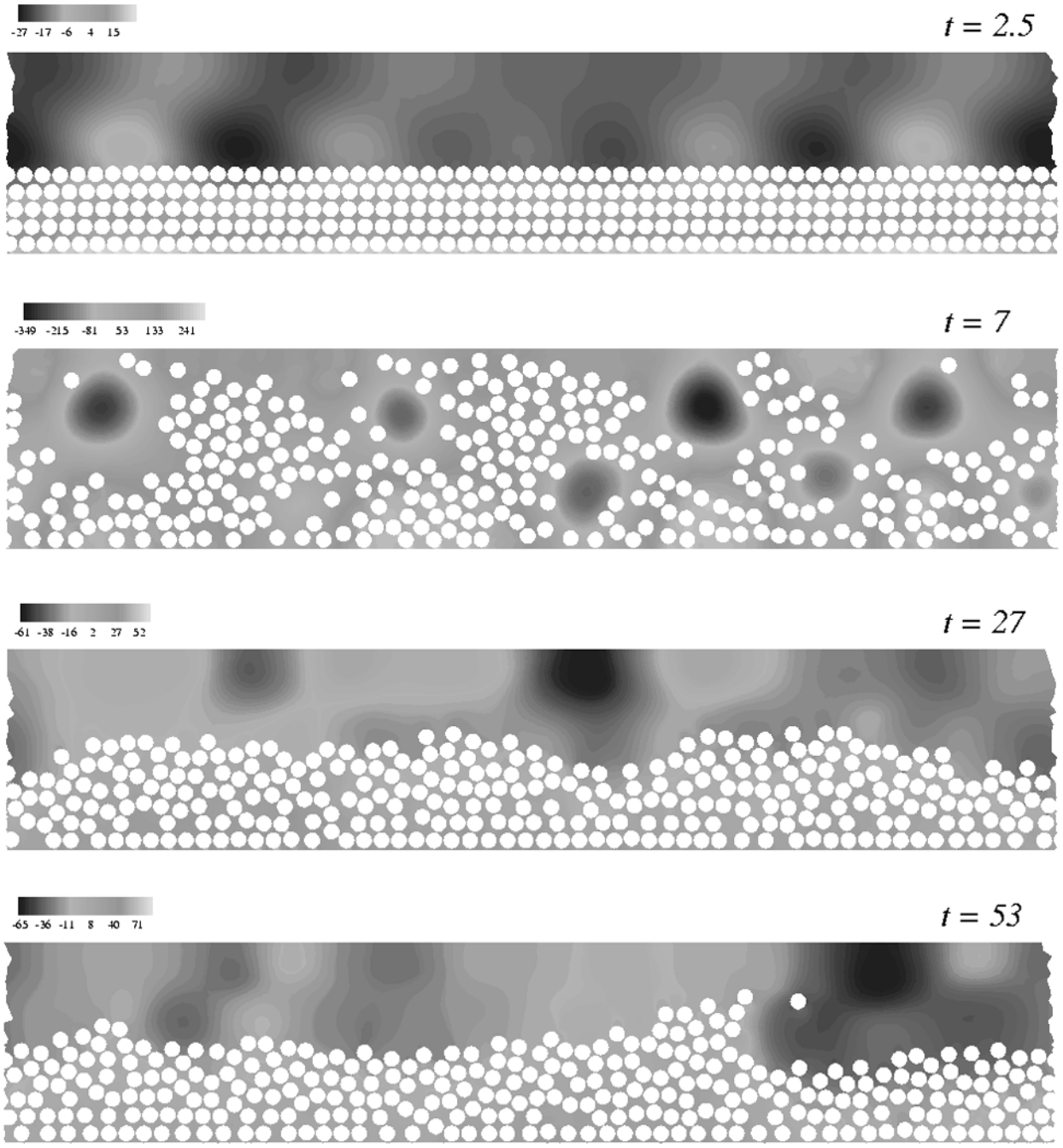

Figure XIV.25. Fluidization of 300 particles (η = 0.05 poise, R = 960, G = 4.09).

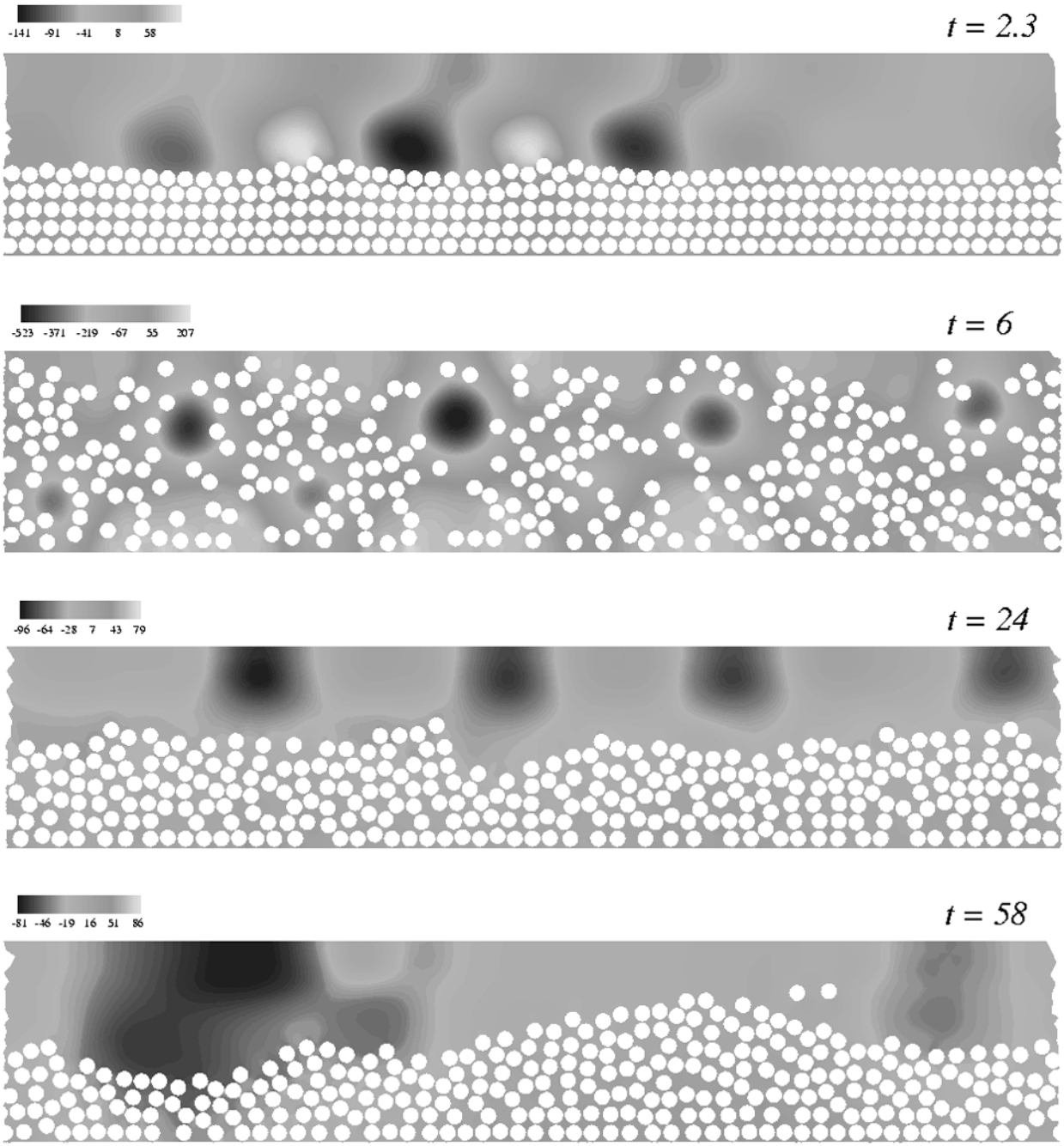

Figure XIV.26. Fluidization of 300 particles (η = 0.05 poise, R = 1200, G = 3.27).

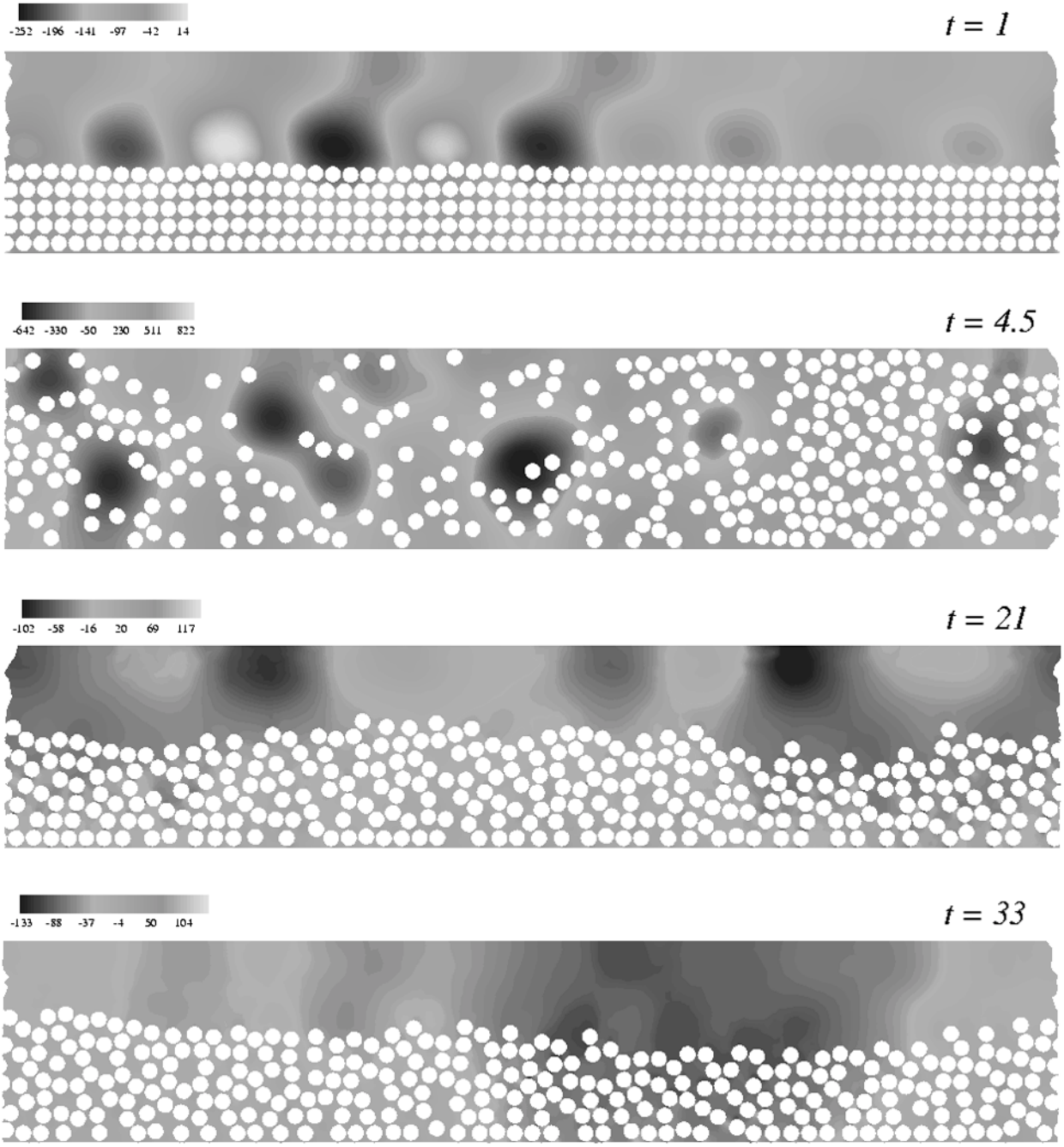

Figure XIV.27. Fluidization of 300 particles (η = 0.05 poise, R = 1680, G = 2.34).

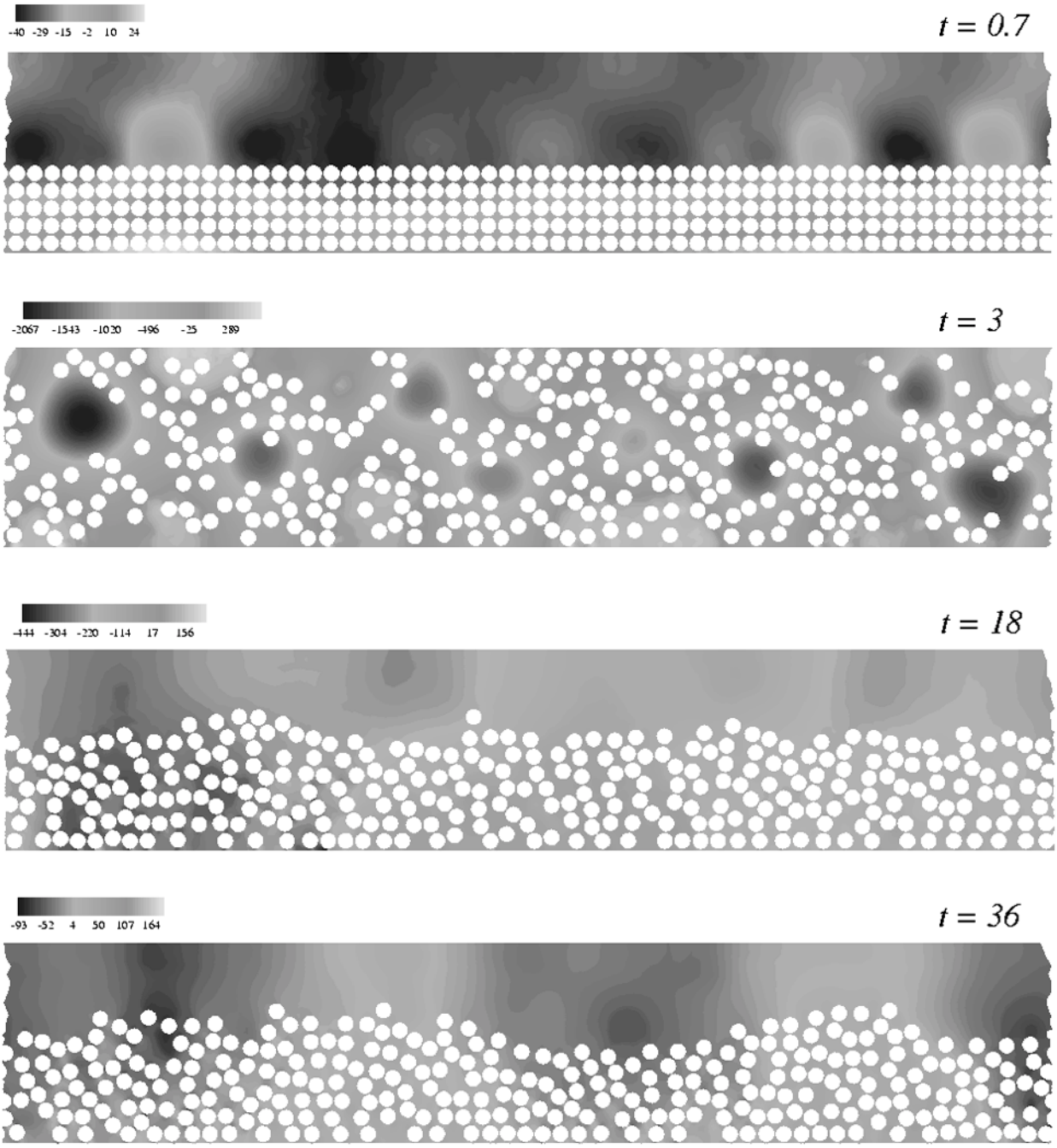

Figure XIV.28. Fluidization of 300 particles (η = 0.05 poise, R = 2400, G = 1.64). The flow is from left to right. The bed rises to the top of the channel where the environment for positive circulation required for lift is unfavorable. The terminal flow is fully eroded and wavy.

▪ Case 5: η = 0.01 poise, $R_G = 9.81/\eta^2 = 9.8\times10^4$

Figure XIV.29 gives the height of center of gravity of 300 particles in water as a function of $R = 6\bar{p}/\eta^2 = 6\times10^4\,\bar{p}$. The interpretation of figure XIV.29 is basically the same as figure XIV.1. Snapshots of the evolution to full fluidization are shown in figures XIV.30 and XIV.31.

The evolution to full fluidization is accomplished by pressure waves. For low Reynolds numbers the bed expansion is small; the snapshot at *t* = 116 sec in figure XIV.30 is an example of bed expansion in water at low *R*. The bed has expanded by the development of voids and dislocations near the top of the bed; only a few particles are fluidized. The bed is not severely eroded.

Fluidization in water at high Reynolds numbers is greatly different. The fully fluidized bed shown at *t* = 0.46 sec in figure XIV.31 is completely eroded. The evolution of the fluidized suspension is driven by a propagating pressure wave, which is in one-to-one correspondence with the propagation of voids. At *t* = 0.27 sec, before the bed has fully fluidized, these voids coincide with wave troughs.

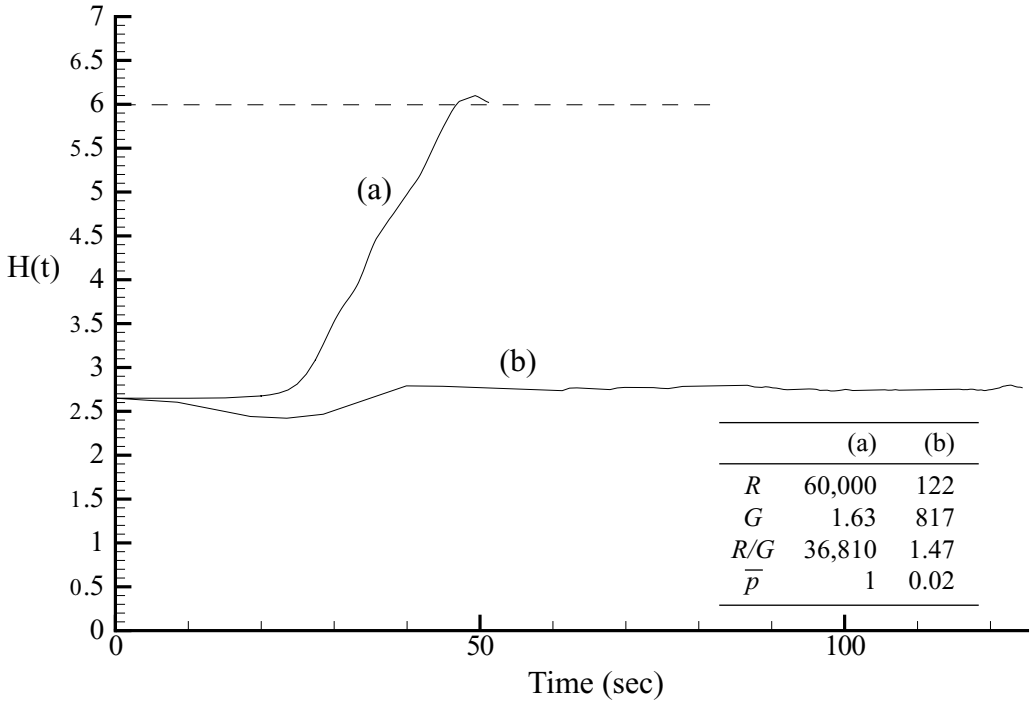

Figure XIV.29. Rise curves for the center of gravity of 300 circular particles fluidized by lift (η = 0.01, RG = 9.81/ η² = 9.81 × 10⁴). $\bar{p}$ is in dyne/cm². The time scale for the fast rise at $\bar{p}$ =1.0 has been expanded by 100; the real time corresponding, say, to 50 is 0.5sec. The rise to full fluidization is very rapid and at full fluidization the mass center of the particles is closer to the top than to the bottom wall. The bed inflation at R = 1200 is modest; at early times the position of the mass center actually decreases because the circles are more efficiently packed. (hexagonally, rather than cubically packed at t = 27.)

Table XIV.5. Data for the forward motion of a fluidized suspension of 300 particles after the bed has fully inflated and the average height $\bar{H}$ of all particles has stopped increasing (η = 0.01). $\bar{H}$ = $\bar{H}_0$ = 2.65d at t = 0. $\bar{U}$ and $\bar{\Omega}$ are the average velocity and angular velocity of particles.

R	G	$\bar{p}$	$\bar{H}$	$\bar{U}$	$\bar{\Omega}$
1200	81.75	0.02	2.77	0.63	0.04
6×10^4	1.64	1.0	6.02	116.20	4.50

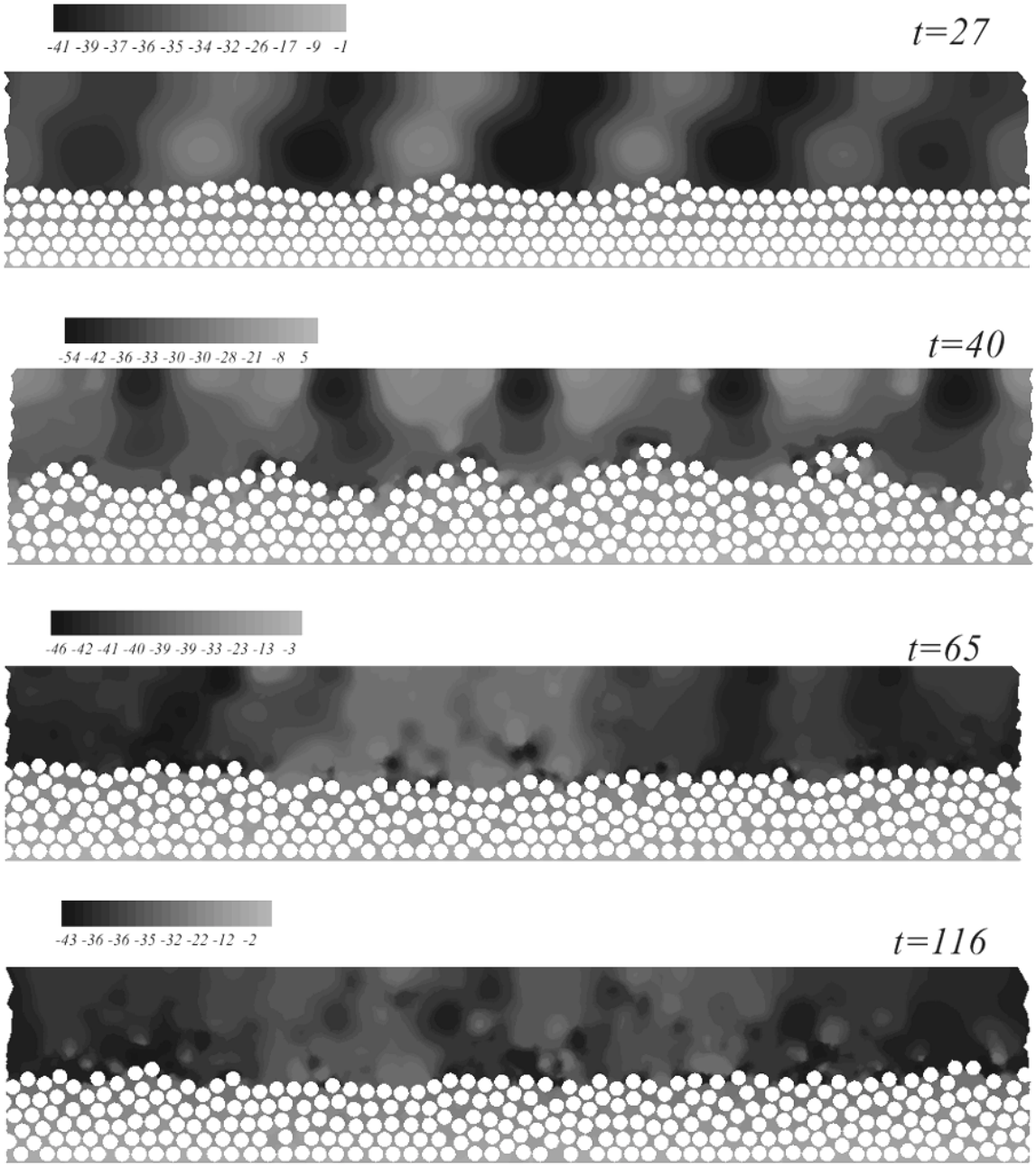

Figure XIV.30. Fluidization of 300 particles (η = 0.01 poise, R = 1200, G = 81.75). The flow is from left to right. This is a "relatively" heavy suspension with a smaller value of R/G. At t = 27 the flow packs the initial cubic array more closely into a hexagonal array and the mean bed height drops. The final fluid condition for t = 116 is mildly inflated, more closely packed at the bottom than the top.

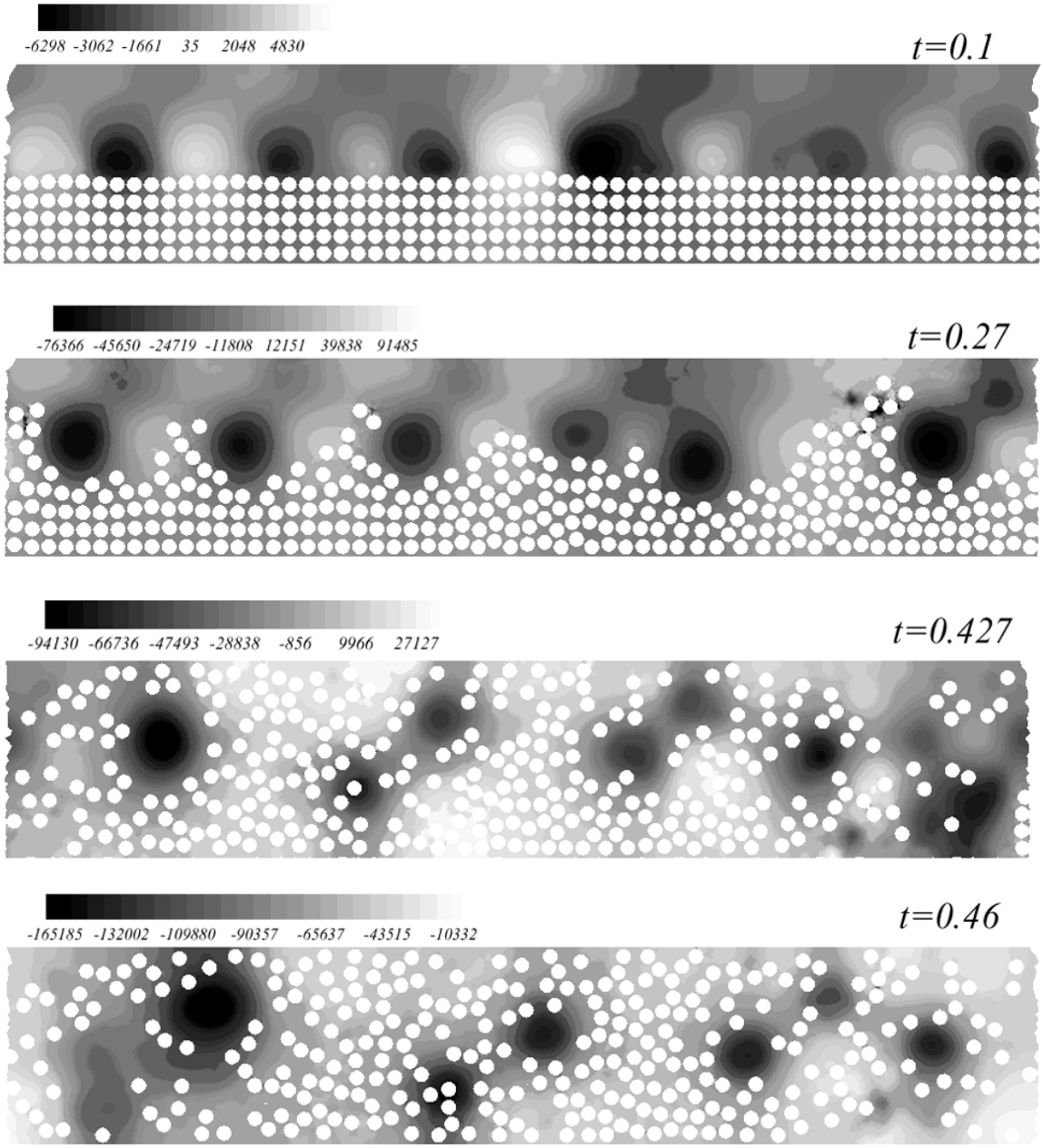

Figure XIV.31. Fluidization of 300 particles in water (η = 0.01 poise, R = 6 $\times 10^4$, G = 1.64), This is a "relatively" light suspension with a much larger value of R/G. Particles fluidize easily; the mean bed height is higher than mid-channel.

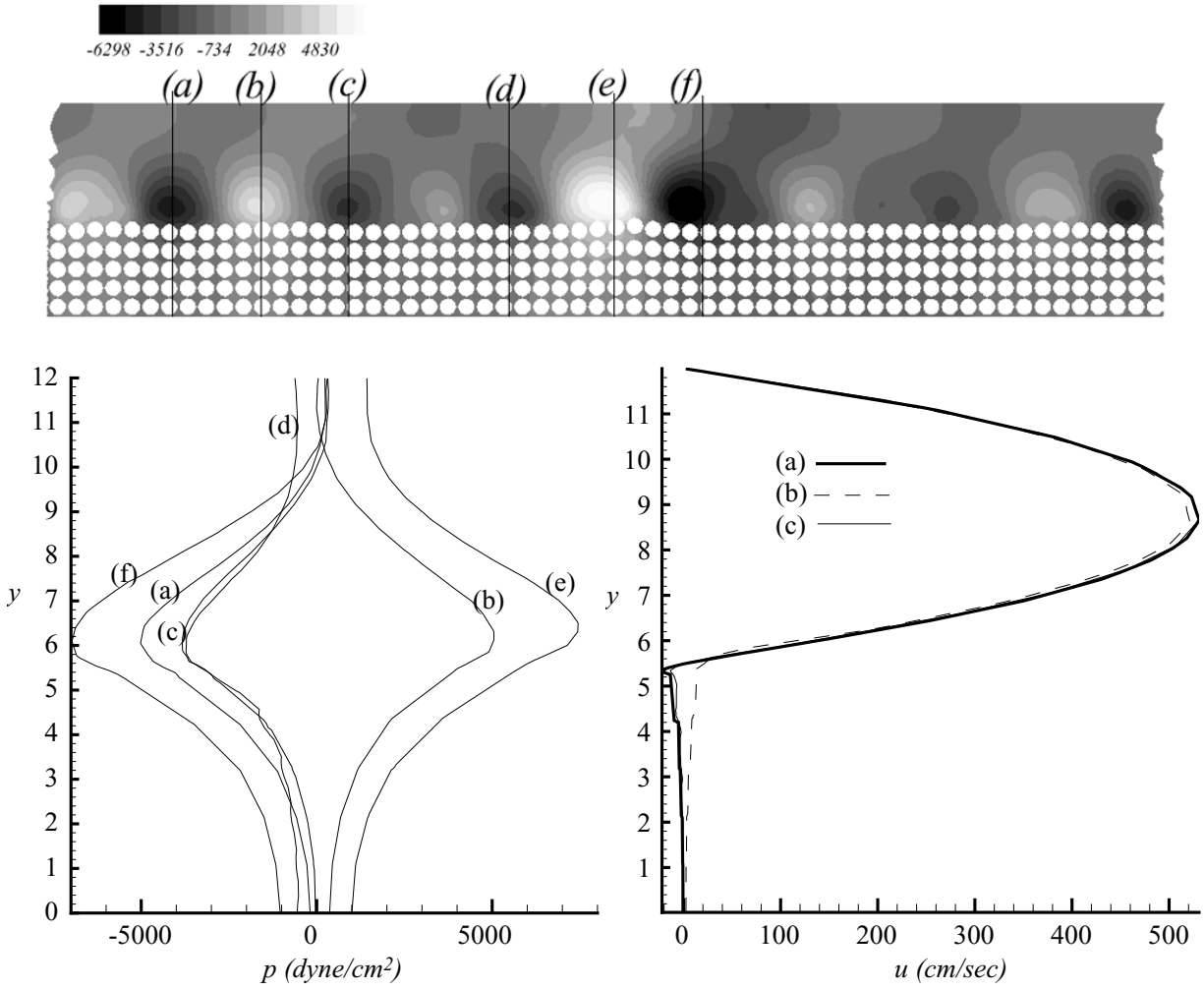

Figure XIV.32. Distribution of dynamic pressure p *and streamwise velocity* u *at* t = *0.1 sec for the fluidization of 300 particles in water when* R = 6×10^4 *(see figure XIV.31). In this case* t = *0.1 sec is not an early time; the propagating pressure wave has already developed, but it does not yet have a big effect on the velocity distribution.*

Figure XIV.32 and XIV.33 show how the dynamic pressure *p* develops as the bed evolves to full fluidization. For this case $t = 0.1$ sec is not an early time; the periodic pressure pulses which drive particles into suspension have already developed.

Figure XIV.34 focuses on the wave properties of the evolving fluidization of 300 particles in water when $R = 1200$. The $t = 40$ sec panel of figure XIV.30 shows a propagating and nearly spatially periodic wave of particles. Wave forms for the dynamic pressure *p*, the vertical velocity *V* and the horizontal velocity *U* are shown.

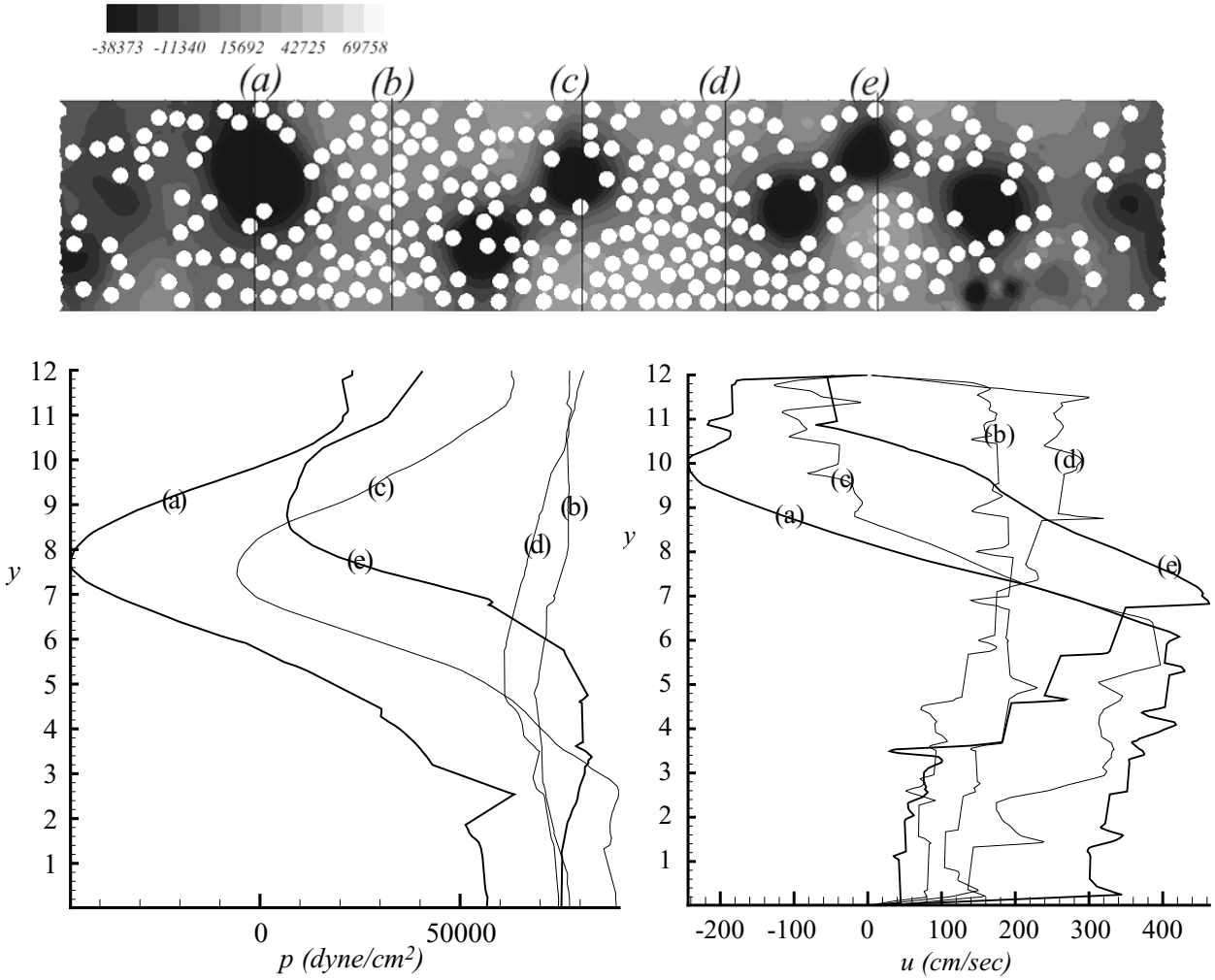

Figure XIV.33. Distribution of dynamic pressure p *and streamwise velocity* u *at* t = *0.46 sec (see figure XIV.31). The pressure and velocity wave coincides with the propagation of internal waves of void fractions.*

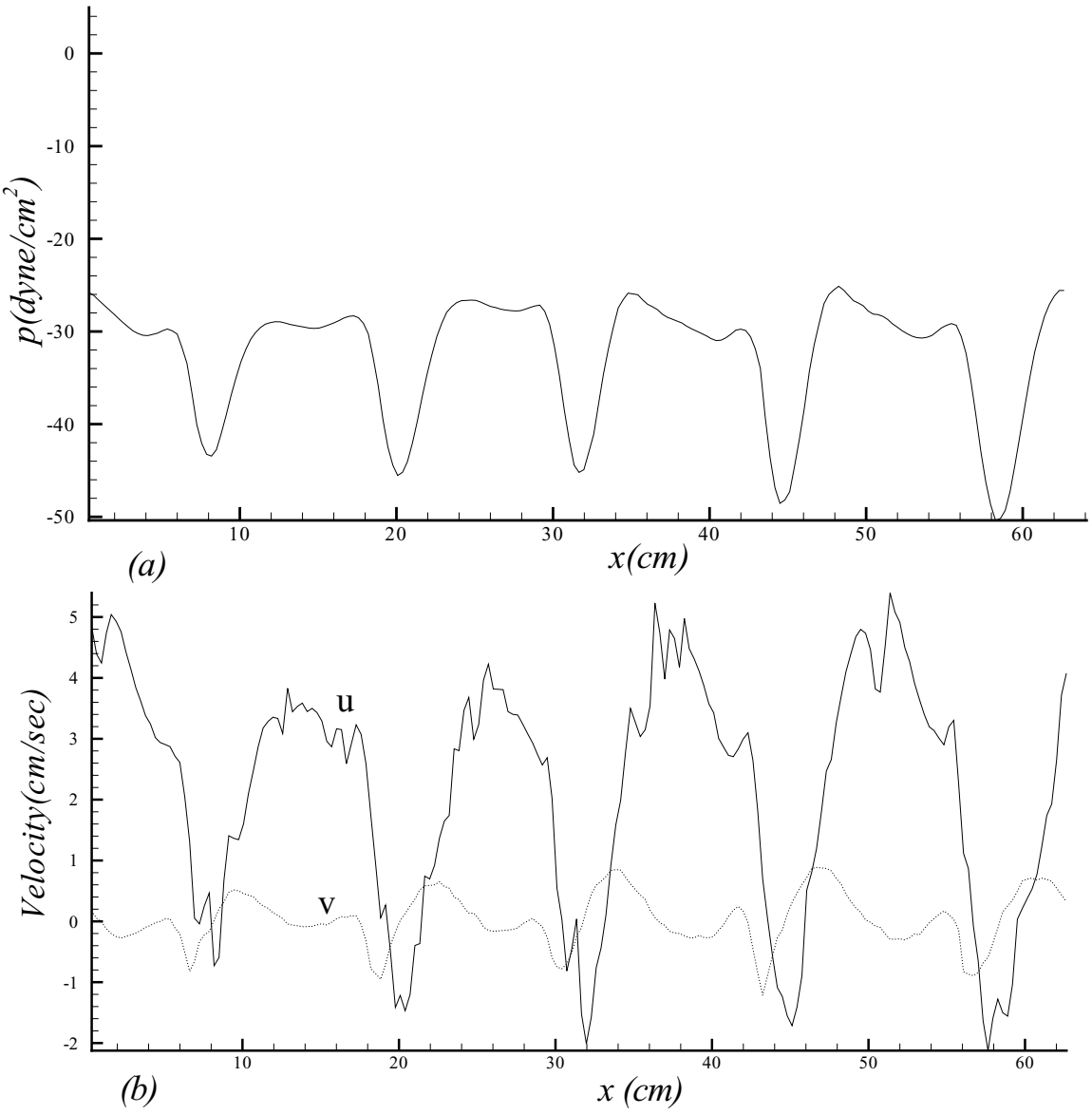

Figure XIV.34. (a) Distribution of dynamic pressure p, *(b) vertical velocity* v *and horizontal velocity* u *in water near the upper wall (*y *= 11 cm) at* t *= 40 when* R *= 1200,* G *= 81.75, see figure XIV.30). These spatially periodic waves propagate.*

▪ An engineering correlation for the lift-off of circular particle in a plane Poiseuille flow of a Newtonian fluid

Choi and Joseph 2001 simulated the fluidization by lift of 300 circular particles in a plane Poiseuille flow of a Newtonian fluid by direct numerical simulation. N. Patankar, Ko, Choi and Joseph 2001 performed similar simulations and reported an engineering correlation for lift-off of many particles in the Poiseuille flow of a Newtonian fluid.

The parameters of the problem are R, R_G, W/d and the average equilibrium height $\overline{H}$ of the bed. We take $W/d = 12$ and $l/d = 63$ for all the simulations. The average fluid fraction ε of the fluid-particle mixture depends on the average height of the bed. The effective weight of a particle

in a suspension is equal to $(\pi d^2/4)(\rho_s - \rho_c)g = \varepsilon (\pi d^2/4)(\rho_s - \rho_f)g$, Foscolo and Gibilaro 1984, Joseph 1990, where ρ_c is the effective or composite density of the fluid-particle mixture. Consequently, the net buoyant weight (or lift) L_s on a particle in a suspension is given by

$$L_s = \varepsilon L = \varepsilon (\pi d^2/4)(\rho_s - \rho_f)g \qquad \text{(XIV.1)}$$

where L is the buoyant weight (or lift) on a particle in the absence of any other particles. We therefore plot εR_G vs. R in figure XIV.35 at different values of fluid viscosities. At a given viscosity the value of R_G is constant. The fluid fraction or the average equilibrium height of the particle bed increased as the Reynolds number is increased. Heavier particles are lifted to a smaller average equilibrium height at the same Reynolds number. We observe that the data at each viscosity can be represented by a power law equation of the form $R_G = cR^m$, where the values of c and m are given in the figure. The value of c varies significantly with respect to R_G whereas the value of m does not show large variation. Figure XIV.36 shows the plot of c vs. R_G on a logarithmic scale. The functional dependence of c on R_G is represented in terms of a power law equation. Combining this result with that in figure XIV.35 we can arrive at a correlation for R_G as a function of R and ε. In figure XIV.37 we reduce all the data points to a single curve. The prefactor in the expression for c is changed from 0.368 in figure XIV.36 to 0.4119 in figure XIV.37 for better agreement between the data and the correlation. The average value of the exponent m is also obtained from the curve fit for all the data points. We get the following correlation for R_G as a function of R and ε

$$R_G = 3.27 \times 10^{-4} \varepsilon^{-9.05} R^{1.249} \qquad \text{(XIV.2)}$$

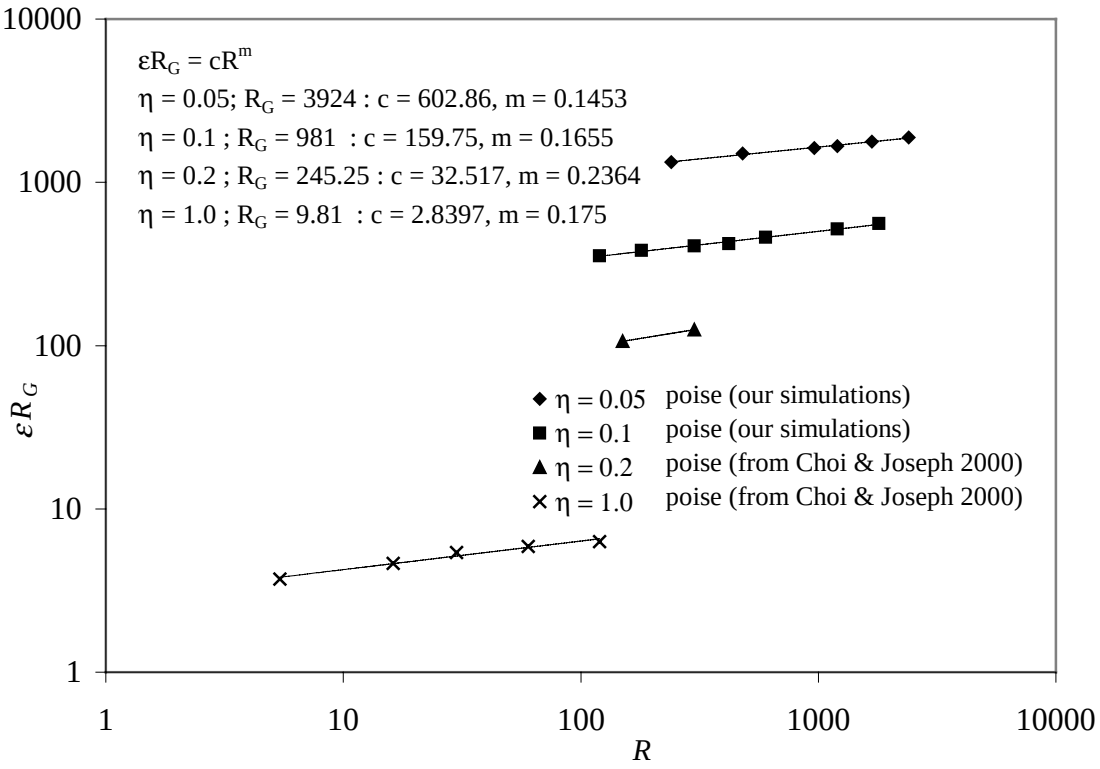

Figure XIV.35. The plot of εR_G *vs. the shear Reynolds number* R *on a logarithmic scale for 300 particles in a plane Poiseuille flow of a Newtonian fluid at different values of fluid viscosities.*

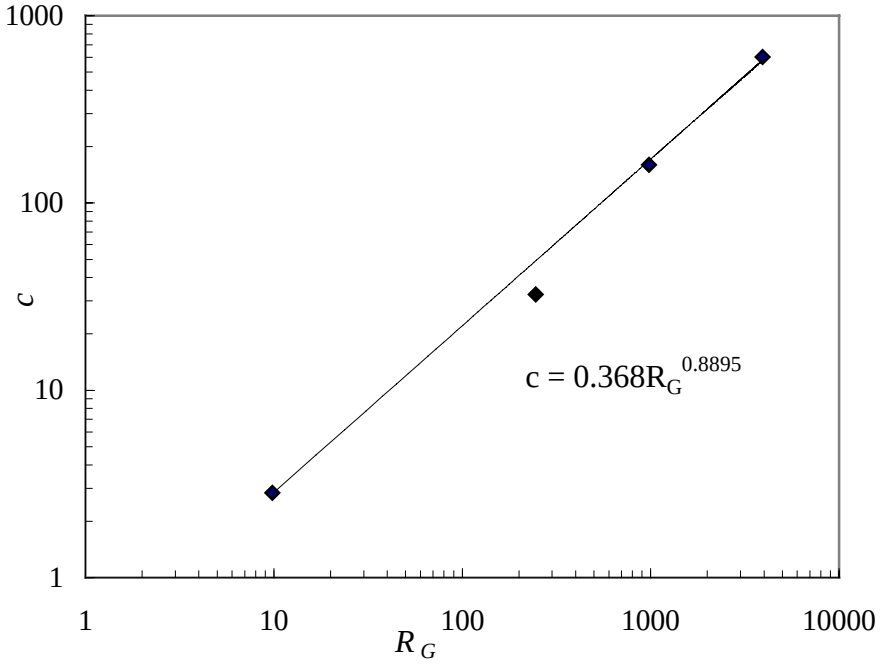

Figure XIV.36. The plot of c *vs.* R_G *on a logarithmic scale.*

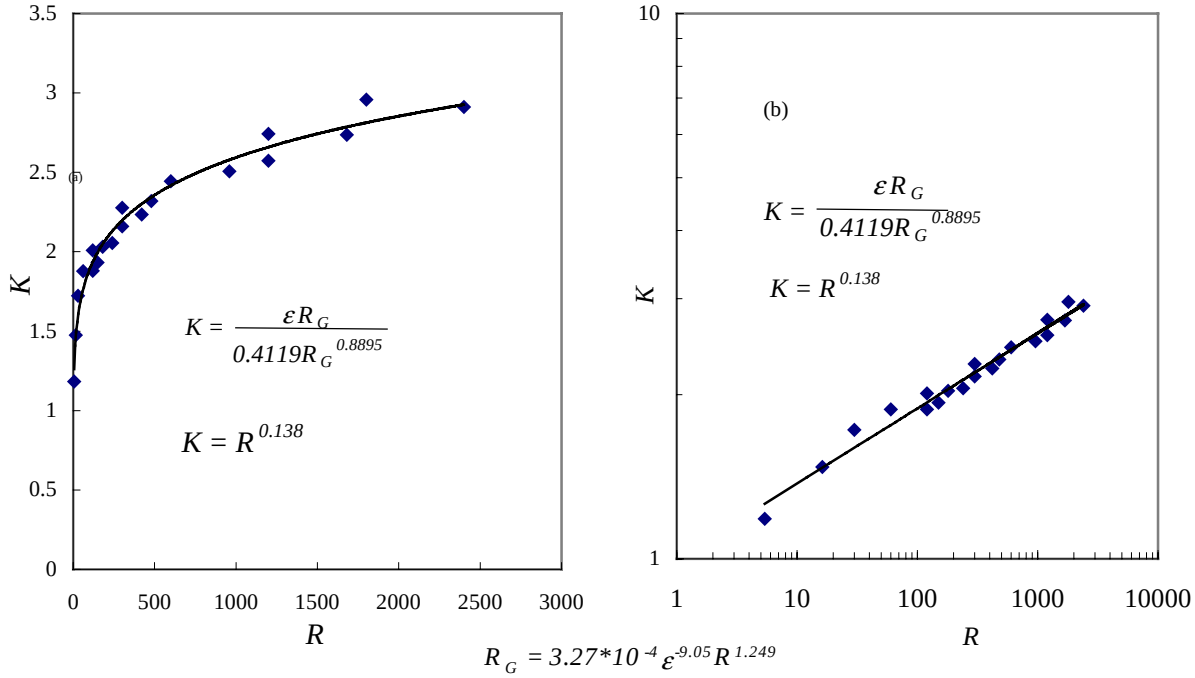

*Figure XIV.37. An engineering correlation for lift-off from numerical simulations of 300 circular particles in a plane Poiseuille flow of a Newtonian fluid (*W/d *= 12). (a) Regular scale (b) Logarithmic scale.*

▪ Inertial mechanism of fluidization

We studied the fluidization of 300 circular particles in a Poiseuille flow. Initially the particles are arranged in a cubic array filling nearly half the channel. The flow breaks the cubic array and inflates the bed by pumping liquid into the bed. The pressures that develop in the bed can levitate the particles. Bed inflation may be divided into two regimes; an eroded bed in which only the top rows of the bed have been inflated, and a fully fluidized bed in which all of the particles are supported by lift forces from the fluid flow. The pumping of liquid into the bed at the earliest times appears to be a universal inertial effect associated with potential flow around spheres and circles. This inertial effect produces high pressure at the front and low pressure at the back side of each circle in the top row of the array. This produces a pressure differential front to back creating a flow into and out the bed, which dislodges particles from the top row. Further fluidization is driven by the development of a periodic wave of pressure and number density which are clearly evident in the snapshots of the bed evolution.

Apart from aspect and density ratios, the dimensionless equations are fully specified by the values of a shear Reynolds number $R = \dot{\gamma} w d^2 / \nu$ and a gravity number $G = d(\rho_p - \rho_f)g / \dot{\gamma}_w \eta$ and the number of particles in the cell. The ratio *R/G* is independent of η and can be viewed as the ratio of lift to buoyant weight whereas the product *RG* is independent of $\dot{\gamma}_w$ and can be regarded as the ratio of buoyant to viscous damping; you get rapid bouncing around when *RG* is large and high lifts, high average height and very inflated beds when *R/G* is large. A summary of the average height, velocity and angular velocity of the particles in the fully inflated beds for η = 1, 0.2 and 0.01 poise are presented in tables XIV.1~4.

We have shown (see figures X.3, 4) that even one particle in a Poiseuille flow can reduce the velocity of the fluid globally; this change is apparently due to the drag of a lagging particle producing liquid holdup. The reduction of the velocity is all the more greater when there are many particles. In figure XIV.38 we have used tecplot to plot profiles at 6 different sections of the flow of 300 particles at $\overline{p} = 20\,\text{dyne/cm}^3$, t = 28 sec identified by vertical lines in figure XIV.5. The open circles give the velocity at fluid points. The straight line segments pass through particles which are rotating. No slip velocity is seen in such a plot; the velocity is continuous through the particle.

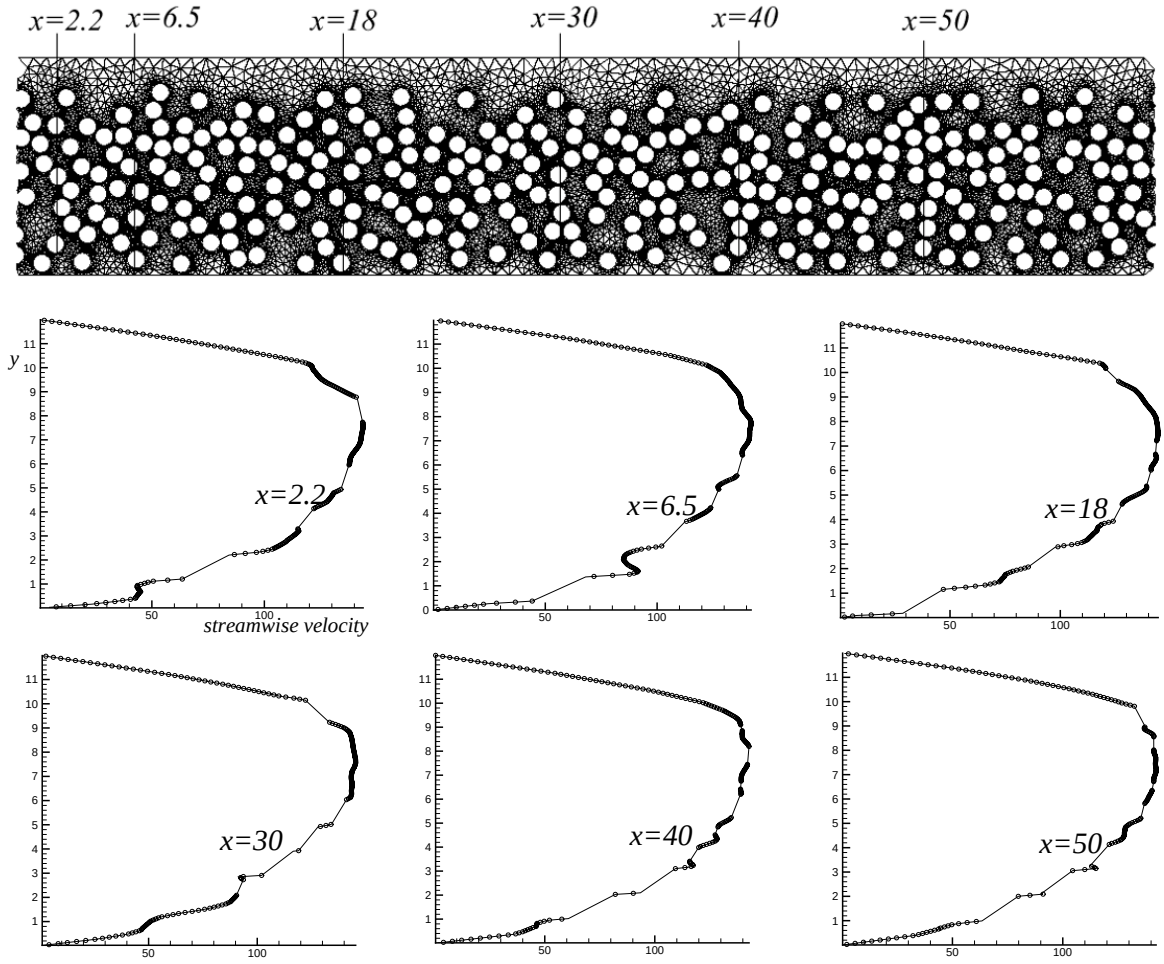

Figure XIV.38. Fluid velocity profiles at 6 different sections of the flow of 300 particles at $\overline{p}$ *= 20 dyne/cm*^{3}*,* η *= 1.0 and when it is fully fluidized (t = 28).*

In figure XIV.39 we plotted the 10 average fluid velocities as a function of *y*. They are obtained by averaging fluid velocities at about 1000 points of *x* coordinate at a fixed *y*. These averages are shown as 10 black circles. A scatter plot of particle velocities is shown and a polynomial fit to this scatter plot is given as a light solid. There does not seem to be a large difference between the average fluid velocity and the average solid velocity defined in this way, but a small positive difference between the fluid and particle velocities is vaguely evident. On the other hand, the difference between the composite fluid-solid velocity and the particle free Poiseuille flow profile is dramatic.

The data shown in figure XIV.39 suggests that one of the main effects of particles in a fluid is to radically reduce the velocity of the composite. Each particle produces a drag on the fluid in a freely moving suspension. The effect of such a distributed drag is equivalent to some form of effective viscosity. Algorithms for the construction of such effective viscosities would find many important applications. Unfortunately the empirical forms of effective viscosity functions which work well for uniform fluidized and sedimenting suspensions work much less well for sheared suspensions.

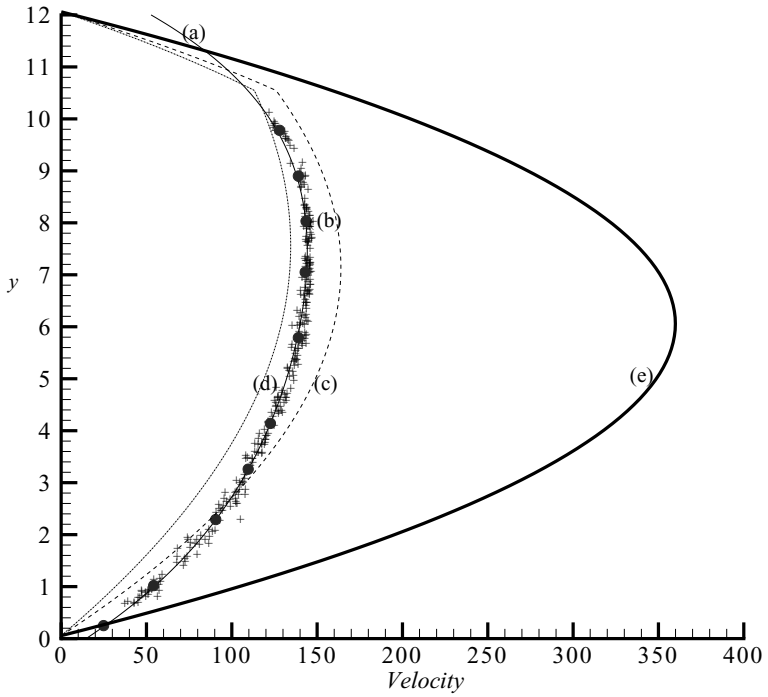

Figure XIV.39. Scatter plot of particle velocities (+) of 300 particles taken from figure XIV.38 (η = 1 poise, $\bar{p}$ = 20 dyne/cm^3); (a) average particle velocity for the scatter (—); (b) average fluid velocity taken from the tecplots in figure XIV.38 at 10 values of y over 1000 points; (c) two-fluid Poiseuille flow model based on (XIV.5) and (XIV.6) using the effective viscosity η_m = 3.06 from (XIV.3) with ϕ = 0.36 and (d) η_m = 4.19 from (XIV.4); (e) undisturbed Poiseuille flow. The particles "hold up" the fluid. The increased drag on the fluid due to the free particles can be modeled as an effect of an increased viscosity of the fluid-solid mixture.

For comparison, we calculated velocity profiles using a two-fluid effective viscosity theory. We suppose that the particle-laden region is an effective fluid with an effective viscosity and an effective density, though the effective density is not needed for the calculation to follow. The selection of the region occupied by the fluid-solid mixture is somewhat arbitrary. We suppose that the mixture has a uniform volume fraction under a flat interface of height $2\overline{H}$ where $\overline{H}$ is the mean height. The volume fraction is obtained as $300\pi d^2/8\overline{H}L$ where *d = 1cm, L = 63cm.* Two highly regarded expressions for the effective viscosity of a uniform suspension of spheres of volume fraction ϕ are:

$$\eta_m = \eta_f/(1-\phi/A)^2,\ A=0.638 \qquad \text{(XIV.3)}$$

which is due to Kataoka et al. 1978 into two dimension and

$$\eta_m = \eta_f (1 + 2.5\phi + 10.05\phi^2 + 0.00273 e^{16.6\phi}) \qquad \text{(XIV.4)}$$

which is due to Thomas 1965. These expressions were obtained from experiments and may not apply in two dimensions. We used $A = A_{2D} = 0.8328$ which scales A into two dimension in the ratio of close packed hexagonal packings in 2 and 3 dimensions $A_{2D} = \frac{0.907}{0.740} A_{3D}$. The effective theory is a two-fluid stratified Poiseuille flow satisfying the following equations

$$\overline{p} = \eta_f \frac{\partial^2 u_f}{\partial y^2} \quad \text{for } y \geq h, \qquad \overline{p} = \eta \frac{\partial^2 u_m}{\partial y^2} \quad \text{for } y \leq h \qquad \text{(XIV.5)}$$

where $h = 2\overline{H}$ is the interface between the pure fluid and the mixture. At the boundary

$$\begin{aligned} &u_f(W) = 0.0,\ u_m(0) = 0.0 \text{ and the velocity and shear stress are continuous on } y = h; \\ &u_f(h) = u_m(h) \\ &\eta_f \frac{\partial u_f}{\partial y}(h) = \eta \frac{\partial u_m}{\partial y}(h). \end{aligned} \qquad \text{(XIV.6)}$$

The comparison of the effective theory corresponding to (XIV.3) and (XIV.4) with the numerical simulation is exhibited in figure XIV.39. The agreement between the effective theory and the simulation is far from perfect but there is agreement within a large tolerance. The effective theory however has several big defects which must be overcome before it can be used to model the slurry; first and foremost the theory requires that *h* be specified; here from the simulation a second problem is that the effective viscosity for uniform suspension need not be a good representation of sheared suspension. It is certain the effective density of the slurry must enter into the height of the fluidized slurry in ways we don't yet understand.

The small difference between the spatially averaged fluid and solid velocities cannot be said to be clearly evident at all positions on a cross section. It is our position that a positive slip velocity is required to support the buoyant weight of particles. In fact, we would expect that the difference between the particle weight and the composite density $\overline{\rho}(\phi) = \rho_p\phi + \rho_f(1-\phi)$ is a factor in the unknown formula for the lift on a particle in a swarm of volume fraction ϕ. In the present case $\rho_p - \overline{\rho}(\phi) = (\rho_p - \rho_f)(1-\phi) = 0.01(1-\phi)$ is very small and a large slip velocity is not required to levitate a particle. The calculation of the slip velocity ought to be defined in terms of time or ensemble averages at a fixed point, which are not readily calculated with the ALE method used here.

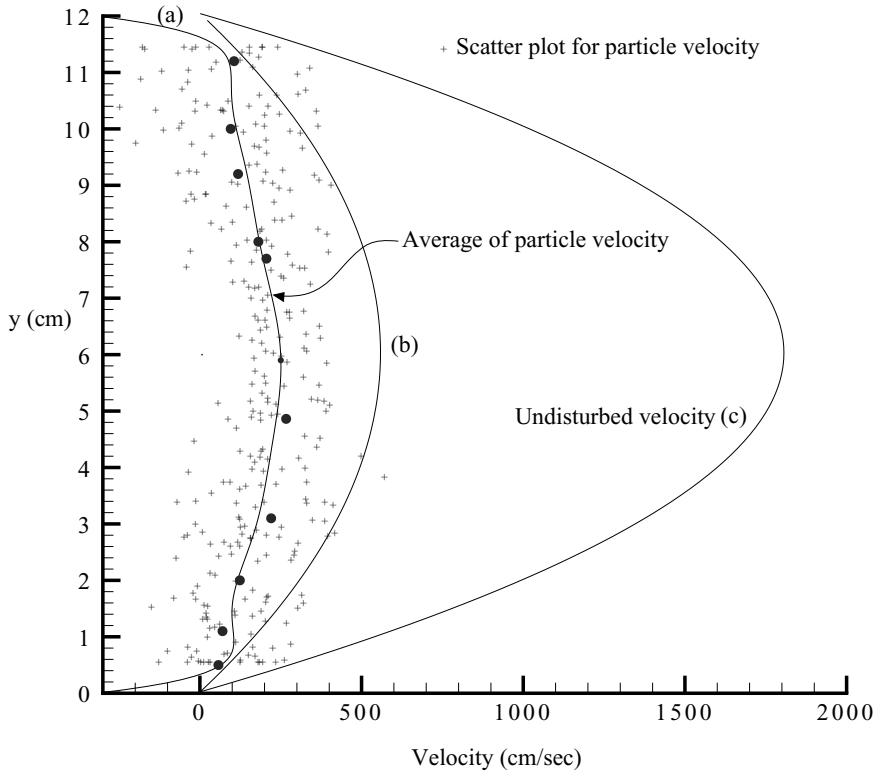

Figure XIV.40. Scatter plot for the fluidization of 300 particles in water (η = 0.01 poise) shown in figure XIV.31. In this case, particles fill the whole channel and the scatter is caused by large fluctuations. (a) The average velocity profile (—) is rather flat as would be expected from turbulent flow. The black dots • are average fluid velocities from the tecplots in figure XIV.31. (b) Velocity profile for Poiseuille flow of a fluid with effective viscosity η_m = 0.032 given by (XIV.4) for ϕ = 0.31. This does not agree with the simulation. Perhaps it would be better to create an effective "eddy viscosity" theory for this weakly turbulent flow. (c) Undisturbed Poiseuille flow without particles.

Figure XIV.40 gives a scatter plot for the water flow in figure XIV.31 (η = 0.01 poise, $R = 6\times10^4$, G = 164). The results here are what might be expected of turbulent flow and appear to represent the natural extrapolation of results given in this paper at lower Reynolds numbers. The relevant Reynolds number, based on the average particle velocity $\overline{U} = 200\,\text{cm/sec}$, the effective viscosity η_m = 0.032 poise and particle diameter d, is about 6000, a value at which one might expect weak turbulence. Informed readers will question the validity of our computation using Choi's 2000 split method in direct numerical simulation with no artificial viscosity or turbulence model. The natural way to test this result is to do mesh refinement. Our unstructured mesh is generated automatically from nodes on the surface of the circular particle. Our calculation converged, and converged solutions have nearly the same height history for 15 to 30 nodes on the circular particle when the time step size (Δt) used is about 10^{-5} (the corresponding Courant number is about 0.1); the converged solution cannot be obtained when the number of nodes is less than 12 or sometimes greater than 30. When the number of nodes is greater than 30, the calculation may stop because the mesh generator is unable to generate mesh due to the distortion of very short elements during motion. Certainly we have not established the validity of such a high Reynolds number computation, but the results do converge to something which appears reasonable and survives tests of mesh refinement.